Chinese Chemical Letters 34 (2023) 108315

Contents lists available at ScienceDirect

Chinese Chemical Letters

journal homepage: www.elsevier.com/locate/cclet

A *trans-ortho* asymmetrically di-strapped metalloporphyrin integrating three key structural features of ligand in heme ☆

Qiuhua Liu[1,*], Junhao Gao[1], Yusheng Zhang, Xin Liu, Xi Zhang, Qin Lin, Wennan Zeng, Zaichun Zhou*

Key Laboratory of Theoretical Organic Chemistry and Functional Molecules, Ministry of Education; and School of Chemistry and Chemical Engineering, Hunan University of Science and Technology, Xiangtan 411201, China

ARTICLE INFO

Article history:
Received 14 January 2023
Revised 22 February 2023
Accepted 7 March 2023
Available online 15 March 2023

Keywords:
Supramolecular effect
Heme analog
Pocket effect
Axial ligation
Ring distortion

ABSTRACT

Heme responsible for the dioxygen fixation, transport and conversion is a metalloporphyrin complex highly dependent on its diverse geometry of ligand. In this work, a *trans-ortho*-di-strapped zinc porphyrin with *dome*-like deformation was synthesized by thermodynamically controlling the formation of *trans*-precursor of porphyrinogen. Its single-crystal structure demonstrated that the asymmetric treatment of porphyrin achieves three goals of creating two secondary coordination sphere (SCS) bulks, maintaining a unique *dome* deformation, and making atomic out-of-plane deviation. In this way, this metallic complex integrates at least three key features of the pocket structure, the differentiated axial ligations, and the ring distortion, making it an ideal heme analog.

Hemes, which mediate numerous biochemical and biophysical processes through its metal center, are one of the most widely used and versatile cofactors employed in biological systems [1]. Metalloporphyrins, as synthetic-based heme analogs [2], have be developed into a powerful tool for studying heme by modifying the periphery and changing the metal center. A number of metalloporphyrin complexes have been generated and used as efficient catalysts in energy conversion [3], chemical synthesis [4], and solar fields [5]. Heme functions are recognized to be highly dependent on their macrocyclic conformation [6] and peripheral geometry [7]. Of these, the pocket structure, the differentiated axial ligation and the ring distortion are three particularly critical structural features (Fig. 1).

Pocket structure usually refer to a cavity on the surface or in the interior of a protein that possesses suitable atmospheres to accommodate ligands [8]. The set of amino acids including its shape and location in the protein around the pocket determines its physicochemical performances and biocatalytic functions [9]. The transport of oxygen (O_2) in hemoglobin is accomplished by the association and dissociation of this gas to its four heme-pockets (Fig. 1, left) [10]. These pockets consist of various amino acid residues [11] responsible for binding and escape of O_2 and H_2O [12]. During the dynamic processes, the architecture and conformation of the pockets, as well as their polarity and pH, will change accordingly. For example, the nonpolar pockets on both faces of the heme-like plane indicates completely reversible oxygenation in the five-coordinate Fe(II) porphyrin complexes, but with significantly reduced O_2 affinity [13]. While pH is closely related to the water migration kinetics [14].

Central iron species have different axial ligation on either side of each heme unit (Fig. 1, middle) [15]. Such difference, albeit small [16], can leads to the completely different binding on both sides. The O_2 species binding on one side are responsible for accepting electron and giving high-valent iron species [17], while the imidazolate character derived from the proximal His-on the other side is responsible for stabilizing the above-mentioned iron species [15] and donating protons to the distal Arg [18], The two types of ligands on both sides have completely different electron effects of pull or push [19], implying the necessity of this axial difference for some heme functions. The difference of the two axial ligations is determined by the macrocyclic deformation and the effect of peripheral substituents [20].

The heme macrocycle hardly adopts a planar conformation (Fig. 1, right) [21]. Heme distortion can significantly affect its key functions closely related to the storage, transport and transform biologically important small molecules, such as O_2 [22], NO [23], and CO [24]. The distortion degree of heme was found to be directly correlated to the electron density and redox potential at its iron

☆ Dedication to Prof. Lixin Dai on the Occasion of His Centenary Birthday.

* Corresponding authors.
E-mail addresses: liuqiuhua@hnust.edu.cn (Q. Liu), zhouzaichun@hnust.edu.cn (Z. Zhou).

[1] These authors contributed equally to this work.

https://doi.org/10.1016/j.cclet.2023.108315
1001-8417/

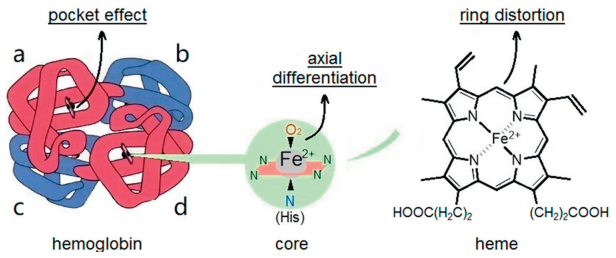

Fig. 1. Three key structural features of heme in hemoglobin.

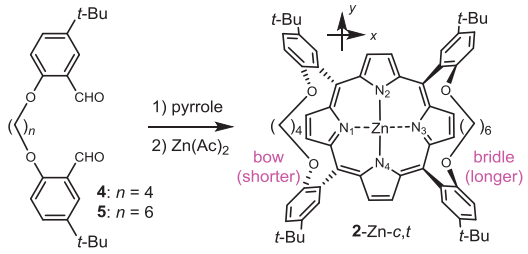

Scheme 1. Synthesis of zinc porphyrin **2**-Zn-*t,o*. The shorter or longer here is based on the size that matches the planar porphyrin, and **2**-Zn-*t,o* denotes the **2**-M-*t,o* (M = Zn) in Fig. 2.

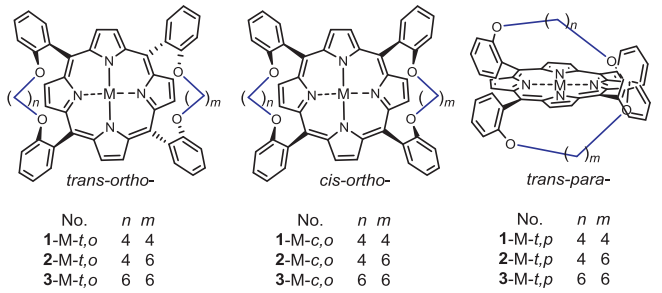

No.	*n*	*m*
1-M-*t,o*	4	4
2-M-*t,o*	4	6
3-M-*t,o*	6	6

No.	*n*	*m*
1-M-*c,o*	4	4
2-M-*c,o*	4	6
3-M-*c,o*	6	6

No.	*n*	*m*
1-M-*t,p*	4	4
2-M-*t,p*	4	6
3-M-*t,p*	6	6

Fig. 2. The possible 9 porphyrin isomers based on the di-strapping strategy. The symbols after each compound number, *c,o*, *t,o* and *t,p*, represent three combinations of *cis-ortho*, *trans-ortho*, and *trans-para* for the two straps, respectively, and all peripheral substituents, like *tert*–butyl, are deleted for clarity.

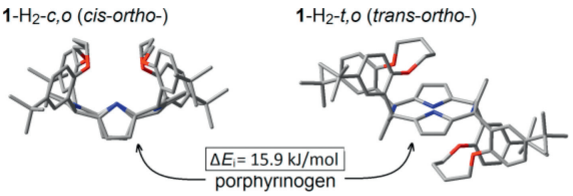

Fig. 3. Comparison of two isomers **1**-H_2-*c,o* to **1**-H_2-*t,o* in total energy. The compound number are defined in Fig. 2.

center [25]. Numerous simulation studies have proved that the role of the ring distortions is mainly in tuning the metallic electronic structure that drives electron transfer [26–28], although these distortions are also possibly involved in maintaining the differentiation of axial ligations [29].

Therefore, we become very interested in designing and developing a heme analog that can integrate these features of pocket effect, axial difference and ring nonplanarity described above in one molecular system. In this paper, we describe the synthesis and characterization of a *trans-ortho*-asymmetrically di-strapped zinc(II) porphyrin complex (**2**-Zn-*t,o*) that stimulates the three key features in heme moiety. The five-coordinate zinc facilitates an observation of the axial difference [30] since only one coordinate site of Zn is exposed to axial binding after offsetting the four sites of porphyrin, and its d^{10} configuration effectively reflects the geometric effect of the ligand because the charge transfer between d orbitals is minimized.

First, the synthesis process and results are discussed. A zinc porphyrin **2**-Zn-*t,o* was prepared according to a locally modified Lindsey condensation [31] and a cascade process [32] of two bridged dialdehydes with pyrrole and zinc salt (Scheme 1). The use of bridged dialdehydes as building blocks can visibly improve the efficiency of cyclization to form porphyrins [33]. Two bridges with different lengths are strapped on both faces of porphyrin plane, respectively, adopting a *trans-ortho*-linked combination. Among them, the shorter bridge acts as a bow at one face of the plane, forcing the ring to deform [34]; while the longer bridge remains relaxed at the other face, without affecting the conformation of the ring [35]. Note that three representative isomers, **1**-M-*t,o*, **1**-M-*c,o* and **3**-M-*t,p* (M = Zn, Fig. 2), were isolated and purified as references. Here, the using of the asymmetric di-strapping strategy is the key to construct the heme-like moiety. The experimental process and characterization are displayed in section 1 of Supporting material.

The key to this synthesis is to pre-fix the nonplanarity of the calix[4]pyrrole intermediate [36], so as to realize the transfer of short bow to porphyrin ring. The real challenge, however, is to improve the relative yield of the *trans-ortho*-di-strapped porphyrins in this synthesis and to separate the target product from possible porphyrin isomers. Some porphyrins based on symmetric di-strapping strategy have been used as molecular devices [35,37] and heme mimics [33]. The Lindsey [31] and Alder-Longo condensations [38] are two general ways for constructing porphyrin skeletons [39]. For the symmetric structures, the number of isomers depends on the three combinations of *cis-ortho* [26,27], *trans-ortho* [33], and *trans-para* [40] of two straps (Fig. 2) but the relative yields of the isomers are significantly different in the two condensations. If two straps with different lengths were used, the isomer number theoretically reaches 9, which will bring great difficulty in separation. Therefore, it is necessary to reveal the reason for the preferential formation of the *trans-ortho* isomer **2**-Zn-*t,o*, and to optimize the reaction conditions accordingly.

The modified Lindsey condensation effectively increases the ratio of the *trans-ortho* porphyrin isomer. It is well known that porphyrinogens, as porphyrin precursors, are first formed under both Lindsey conditions and Alder-Longo ones [36]. Therefore, conditions favorable for forming the porphyrinogens can be considered as those favorable for forming the corresponding porphyrins. Density functional theory calculations were carried out at B3LYP/6-31G level [41] to evaluate the thermodynamic stability of isomers. Results indicate that *trans-ortho*-di-strapped porphyrinogens are thermodynamically more stable than the *cis-ortho*-forms (Fig. 3), although the rule is reversed for the relative di-strapped porphyrin units [33]. When the straps are $O(CH_2)_4O$, the total energy (E) of the *trans-ortho*-di-strapped porphyrinogen (**1**-H_2-*t,o*) is 15.9 kJ/mol (ΔE_i) lower than that of the *cis-ortho*-form (**1**-H_2-*c,o*), this difference ΔE_i is near the maximum value of 2∼16 kJ/mol similar to the *cis-trans* isomers [42,43], suggesting a clear thermodynamic control mechanism for increasing the ratio of the *trans-ortho* isomer in current modified Lindsey method [44]. Note that when the straps become longer $O(CH_2)_6O$, the ΔE_i between the two isomers increases to 34.9 kJ/mol, indicating a better thermodynamic control effect (Fig. S7 in Supporting information).

For the two condensations, besides the different catalysts used, another key difference is the reaction temperature. The Lindsey condensation occurs at room temperature or lower, about 100 °C lower than in Alder-Longo condensation, thus the Lindsey condensation tends to afford thermodynamically stable isomers. The results have shown that the overall yield of the *trans-ortho* isomers

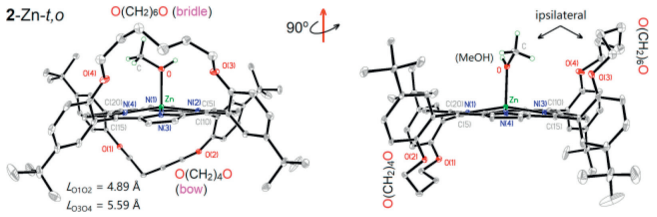

Fig. 4. Ipsilaterality of axial ligands to longer ether chains in **2**-Zn-*t,o*. All hydrogen is omitted except for that on the ligand for clarity.

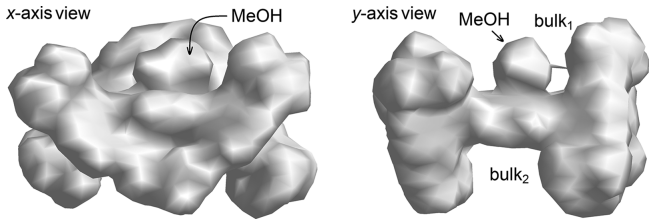

Fig. 5. Total charge density surface of zinc porphyrin **2**-Zn-*t,o*. View along x-axis (top) and y-axis (bottom).

is much higher than that of the other two isomers of the *cis-ortho* and *trans-para* under the modified Lindsey conditions. Thus, the *trans-ortho*-isomer **2**-Zn-*t,o* is easily purified by multiple recrystallizations followed by careful column chromatography.

Secondly, the structures similar to heme are discussed. The zinc complex **2**-Zn-*t,o* was determined by single crystal X-ray at 113 K. The solid structure is displayed in Fig. 4. As can be seen, two ether straps, -O(CH_2)$_6$O- and -O(CH_2)$_4$O-, are arranged on two opposite faces of the porphyrin plane. The longer strap acts like a soft bridle in bridled porphyrin [45], and its O–O distance reaches 5.6 Å, has little effect on the plane conformation, while the shorter strap makes the molecule tense up, and its O–O distance is shortened to 4.9 Å, making the porphyrin core deformed. For Zn ion, the receptor site form five-coordinate square pyramidal complex by axial ligation of methanol [46]. The complex vividly reflects the three features of pocket structure, differentiated axial ligation, and ring distortion in hemoglobin.

The so-called heme pocket is a cavity composed of amino acid residues flanking the heme plane [47]. The pocket created open microenvironment around the heme iron center [48] to manipulate the binding of oxygen and the release of water [20,49]. In this way, the pocket must possess or acquire several features that complement those of potential guests. Specifically, the volume and shape should match that of ligand, and the polarity should favor the binding of non-polar binder [50].

The pocket effect of heme falls under the category of the secondary coordination sphere (SCS) and determines many key physical and chemical properties of hemoglobin [51]. The SCS effect refers to the interactions of metal and its primary ligands with groups that are not part of the intimate coordination environment of the metal [52]. It impacts almost all aspects in transition metal-mediated processes [53], and is widely used to explain catalytic processes such as CO_2 reduction [54,55] and oxygen-atom transfer [56]. Much research has been done on modification of porphyrin complexes to mimic the SCS moiety of natural heme [57–59,28].

For the asymmetric **2**-Zn-*t,o*, its two straps and four *tert*–butyls form its SCS entity. Compared with the reported "picket fence" and "double bow" complexes, the asymmetric complex possesses at least three interesting SCS advantages, as shown in the total charge density surface maps (Fig. 5). (a) **2**-Zn-*t,o* includes two relatively stable SCS bulks unaffected by solvent effects and molecular motions [60], thanks to the covalent bonding of the two straps with two pairs of *meso*–aryl groups, respectively. (b) The two SCS

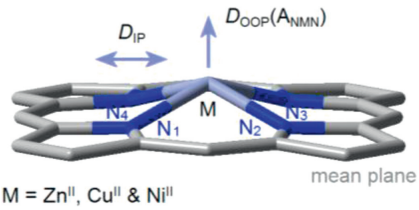

Fig. 6. *dome*-type metalloporphyrin models. D_{IP} and D_{OOP} represent the degree of in-plane (IP) and out-of-plane (OOP) deviations, respectively, A_{NMN} denotes the bond angle of N_1MN_3 or N_2MN_4.

bulks (bulk$_1$ and bulk$_2$) are located on both faces of the porphyrin plane, exactly matching the requirement of the two axial ligations of heme center [15,17]. (c) Each SCS bulk consisting of a four-walled, half-ball pocket sphere is large enough to accommodate the small molecules such as O_2, NO, and CO, and amino acid residues, such as the imidazolyl of His-or the mercapto of Cys, since the methanol ligand completely immersed in the current bulk of **2**-Zn-*t,o* is larger in size than the aforementioned substrate molecules. In addition, keeping the SCS bulk in hydrophobicity is also its key feature, which is very beneficial for the circulation of reactive oxygen species in the pocket [10], because the hydrophobicity is the best driving force for the exchange of O_2 and H_2O. In order to further highlight the advantages of the *trans-ortho*-di-strapped complex in mimicking heme, another three symmetrical di-strapped zinc materials, **1**-Zn-*t,o*, **1**-Zn-*c,o* [61] and **3**-Zn-*t,p*, were separated and collected as references, where *t,o*, *c,o* and *t,p* represent the *trans-ortho*, *cis-ortho*, and *trans-para* combination of two straps, respectively, and three single crystal structures and relative molecular surface figures are shown in Figs. S1 and S14 (Supporting information), respectively.

These three reference complexes show their advantages and disadvantages as heme mimics. Among them, **1**-Zn-*t,o* is the most similar to **2**-Zn-*t,o* in structure, and its two SCS bulks are stable and large enough in size, but its disadvantages lie in the lost axial dissimilarity and the fixed ring geometry. **1**-Zn-*c,o* can only provide a decent bulk due to the *cis-ortho* combination of the two straps. While **3**-Zn-*t,p* cannot give SCS bulk due to complete obstruction by its two straps. These comparisons indicate that the other two *cis-ortho*-di-strapped porphyrin complexes and two *trans-para*-di-strapped ones (Fig. 2) have even less plausible as heme mimics.

The differentiation is shown by different axial ligation on both faces of heme, and the both faces are responsible for accepting electron-donating ligand like His residues and binding electron-withdrawing one like O_2 respectively [15,17], which is doomed to be different for the two axial sites of center metal. For tetrapyrrole complexes, a size-matching between the N_4 core and the complexed metal must be met as far as possible [62,63]. On the one hand, if the metal is too large or too small in diameter, the tetrapyrrole will adjust its core size to adapt to the metal species through ring distortion [64] or reduction [65]; on the other hand, If the core diameter changes, the metal will be sized accordingly to suit the deformed core [66]. In these mutual matching processes, the in-plane (IP) and out-of-plane (OOP) deviations of the central metal are inevitable (Fig. 6).

The OOP deviation of central metal can be considered as the key to the axial differentiation. The IP deviation has been confirmed to tune the axial affinity through the core breathing mode [22], which obviously does not cause the occurrence of the above axial differentiation. An inspection in Fig. 6 shows that the metallic OOP effect causes all four pyrrole units to tilt in the same direction, forming a *dome* structure [67]. This *dome* motif represents one of several typical motifs, such as *saddle*, *ruffle* and *dome* that have been clearly identified in the heme [21]. In general, the *dome* structure can be induced by large metal ions, such as lanthanides [68],

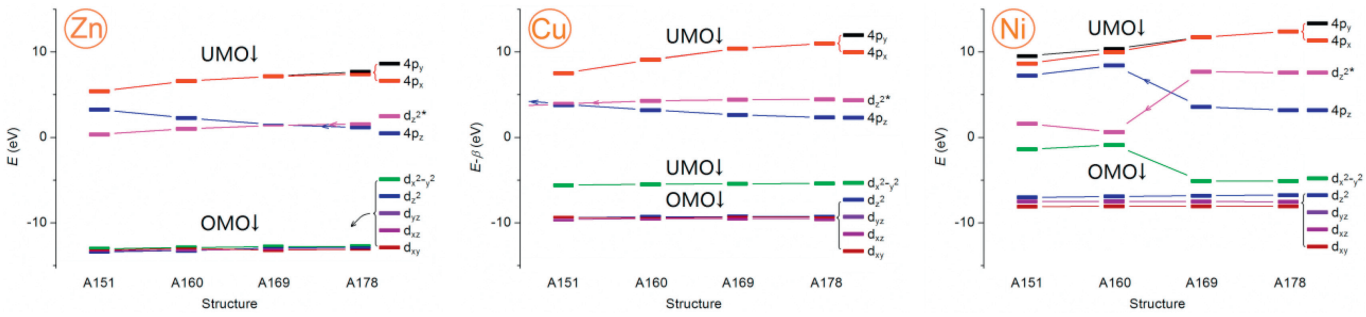

Fig. 7. The relative energy (E) of 4p and 3d orbitals of metal Zn, Cu and Ni with increasing distortion when the diagonal N-M-N bond angle in core is from 178° to 151°. UMO and OMO represent unoccupied and occupied molecular orbitals, respectively.

or square pyramidal transition metal ions, such as iron in heme [69]. However, unlike the *saddle* and *ruffle* structures [28,40,61,68], it is still unclear how the *dome* deformation affects heme functions [62].

DFT calculations were carried out to intuitively quantify the impacts of metal OOP on axial differentiation, thus revealing the origin of the axial ligations. Therefore, three metalloporphyrin complexes containing metal (M = Zn^{II}, Cu^{II} and Ni^{II}) were constructed as models by continuously changing the out-of-plane degree (D_{OOP}) of metals. For comparison, the D_{OOP} value is quantified by continuously controlling the two diagonal N-M-N bond angles (A_{NMN}) in the core, ranging from 178° to 151° in 9° steps. In this way, for each metal, four model structures are optimized. The energy (E) of 9 orbitals, including five bonding 3d, one anti-bonding 3d (*i.e.*, $3d_{z^2}$*) and three 4p, is collected in each metal, as shown in Tables S4–S6 (Supporting information), and the plots of these orbital energies (E) to the bond angle (A_{NMN}) are displayed in Fig. 7. Note that Cu^{II} and Ni^{II} ions are used here as the references of Zn^{II} specie to observe the OOP effect due to the comparability of their anti-bonding d orbitals.

The OOP effect of 9 orbitals is revealed by plot of its E and respective OOP values, where the OOP is represented by the A_{NMN}. The four main trends are as follows: (1) The E of the anti-bonding unoccupied molecular orbitals (UMO) is related to the OOP value of metals, while that of the bonding occupied molecular orbitals (OMO) is almost independent of the OOP value; (2) For four UMOs, p_x, p_y, p_z and d_{z^2}*, the E of the two axial UMOs, p_z and d_{z^2}* intersect with the increase of the OOP value, while that of the other two UMOs, p_x and p_y, decreases continuously in this process. (3) For different metals, the E intersection of p_z and d_{z^2}* occurs in different OOP scopes, which are <178° for Zn, <151° for Cu, and <169° for Ni expressed by bond angle (A_{NMN}). (4) For equatorial $d_{x^2-y^2}$ orbital, its E change depends on its charge number. The E of full filled or half filled $d_{x^2-y^2}$ form is almost unchanged in Zn or Cu-β model, and that of empty $d_{x^2-y^2}$ produce an energy jump of 3.7~4.5 eV in Ni models. In short, the E of the two axial UMOs and one equatorial UMO has obvious OOP effect. It should be pointed out that the E change of equatorial $d_{x^2-y^2}$ can tune the direction of LMCT in metalloporphyrins, but it does not directly cause the axial differentiation [28].

Similar to the changes in orbital energy (E), those in orbital shape are mainly reflected in the two axial UMO orbitals. The molecular figures of two UMOs in current three complex models and the comparison of molecular figures of all 9 orbitals in each metal are placed in Figs. S10-S13 (Supporting information). Comparison showed that (1) the OOP effect makes the two UMOs asymmetric, and the asymmetry is manifested in the orbital disproportionation on both sides of the plane, that is, the increase/decrease of volume/density on one side of the orbitals is caused by the decrease/increase of volume/density on the other side of the orbitals, and *vice versa*, the disproportionation degree

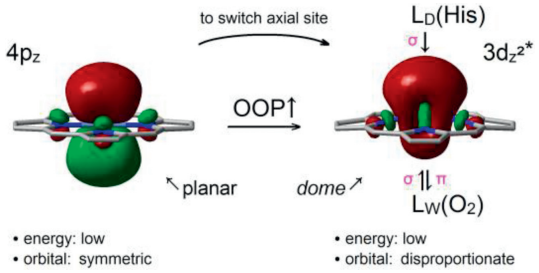

Fig. 8. The energy intersection and the orbital disproportionation induced by metallic OOP effect. L_D and L_W denote electron-donating ligand such as His-and electron-withdrawing one such as O_2, respectively.

positively correlated to OOP values, (2) the shape variation range of d_{z^2}* is much larger than that of p_z. For d_{z^2}*, the branch on the side of OOP has become dominant in volume when A_{NMN} < 160°, while for p_z, the branch on this side only slightly increases. (3) The disproportionation degree becomes more and more significant from Zn^{II} to Cu^{II} to Ni^{II}, suggesting that the electron vacancy in valance orbitals has a positive contribution for the disproportionation.

The OOP effect of metals has been fully analyzed in terms of the orbital energy and shape in above, which proves that it is these two axial UMOs that determine the type and degree of axial ligation, regardless of whether the two orbitals belong to frontier molecular orbitals due to the need of coordination direction. The analysis can clearly delineate the role of *dome* deformation (Fig. 8) in nonplanar metalloporphyrins [66]. On the one hand, the decrease of the d_{z^2}* orbital energy switches the axial ligation site from p_z to d_{z^2}* and strengthens the ligation effect due to the energy intersection of the two UMOs caused by OOP effect, and the axial ligation with the lower d_{z^2}* orbital is more conducive to the ligand-to-metal charge transfer (LMCT).

On the other hand, in the d_{z^2}* orbital of *dome* model (Fig. 8, right), the orbital disproportionation made the ipsilateral branch of OOP significantly expand and the opposite branch significantly shrink, respectively. The expanded branch can visibly enhance the attraction to electron pairs due to the increase of orbital vacancy and volume, which makes it more likely to accept electron-donating ligand (L_D) such as His residues. While the shrunk branch can greatly shorten the distance from d(M) to π(L) forming d-π feedback bond, which enables it to more firmly bind electron-withdrawing ligand (L_W), such as O_2, where $d = d_{x^2-y^2}$. The feedback bond is essential for the stability of Chatt-type oxygen complexes [62].

The ring distortion (also expressed as nonplanarity and deformations in different reports) is a conserved feature of natural tetrapyrrole complexes [70] such as heme [71]. There are many researches related to the distortion, which can be summarized to

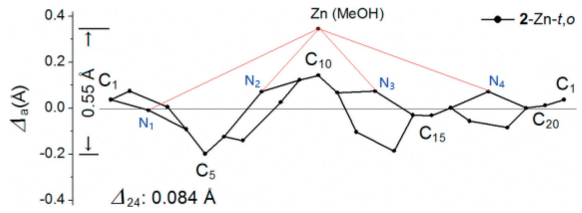

Fig. 9. Ring distortion represented by atomic displacement (Δ_a) in **2**-Zn-*t,o*. The diagram begins with $C_{1\text{-}\alpha}$ and finish at $C_{20\text{-}m}$ atoms.

reveal its roles at least from the following three aspects: (1) Adjust the coordination geometry and d orbital energy of the complexed metal by changing the core diameter to promote electron transfer between metal and the axial ligand [26,27,72]; (2) Tune the relative energy of the frontier molecular orbital in metal and porphyrin to switch the direction of electron transfer between the metal and the horizontal ligand [28,33], which is particularly important for the photosynthetic system; (3) Differentiate the ligation environments of two sides to bind different ligands, as described in the previous section of this article. The summary indicates the necessity of ring distortion in those enzymes containing metallic tetrapyrrole.

The tetrapyrrole ring of **2**-Zn-*t,o* shows the *dome*-like core deformation, which meets the metal OOP required by the heme (Fig. 4). The model molecule is di-strapped by a "bow" and a "bridle", but only the short bow contributes to the ring distortion from one face, while the long bridle contributes negligible from the other face. Several bond parameters involved to the core moiety of **2**-Zn-*t,o* are shown in Table S2 (Supporting information). Comparisons show that (a) the Zn ion deviates from the core plane, as manifested by two facts: the sum of two Zn-N bond length, *L*(Zn-N), is larger than the distance of diagonal N–N, *L*(N–N), and the *L*(Zn-N) is slightly longer than that in the planar porphyrin; (b) the core deformation is asymmetric, as evidenced by the following facts: $L(N_1\text{-}N_3)$ is 0.07 Å shorter than $L(N_2\text{-}N_4)$, and the torsion angle of four *meso*–C and four core N is up to 4.5° [$D(C_4)$] and 1.6° [$D(N_4)$], respectively; (c) the OOP degree of current Zn ions reaches or exceeds the level of energy intersection of two UMOs of Ni or Zn ion in relevant models (Table S2), as proved by 162°–165° of A_{NZnN} in **2**-Zn-*t,o*.

The tetrapyrrole ring of **2**-Zn-*t,o* shows the distortion of the ring itself, which leads to the narrowing of LUMO-HOMO gap that causes a bathochromic spectrum [33] and the reduction of LUMO (a_{2u}) energy that facilitates metal-to-ligand charge transfer (MLCT) in heme [26,73]. Quantitative displacements of each atom in **2**-Zn-*t,o* complex (in units of Å) from the 25-atom mean plane and the diagram illustrating the ring conformation are given in Fig. 9 and Table S3 (Supporting information) of supporting material, respectively. The ring distortion is specifically shown as that (a) almost all atoms deviate from the 25-atom mean plane; (b) the two atoms with the largest displacement are Zn and C_5, with Δ_a values of 0.35 and −0.20 Å, respectively, and the sum of the absolute distance between the two is 0.55 Å; (c) the total displacements of the ring is 0.08 Å.

The ring distortion marked by the atomic displacement will narrow the LUMO-HOMO gap [33], at the same time, the narrowing will be represented by the spectral red-shift. The red-shift phenomena of the nonplanar porphyrins were extensively demonstrated and explained by hybrid orbital deformation (HOD) effect [74]. As expected, the maximum absorption of **2**-Zn-*t,o* is 430 nm, which has a red shift of 12 nm compared with the planar zinc porphyrin, as shown in Fig. S15 (Supporting information), where the planar reference is 5,10,15,20-tetraphyenl zinc(II) porphyrin (TPPZn). This shift amplitude is close to that in natural heme [75], but it is smaller than the ~25 nm red shift in the nonplanar system previously reported by our research group [33,74], which means that it is very promising to obtain heme models with greater distortion range.

In this work, a *trans-ortho*-di-strapped zinc porphyrin **2**-Zn-*t,o* with *dome*-like deformation was synthesized, characterized and studied as heme mimic. The values of this work include: (1) The synthesis of the asymmetric complex is realized by utilizing the thermodynamic difference of the porphyrinogen *trans/cis*-isomers; (2) The single crystal structure presents the SCS effects of peripheral groups on both sides; (3) DFT results of the *dome* metalloporphyrin models quantify the effect of metallic OOP effects on axial differentiation; (4) The quantitative displacement of each atom in the complex from the mean plane intuitively shows the way and amplitude of ring distortion. In this way, the three key features of pocket structure, differentiated axial ligation and ring distortion in heme were integrated in one molecule. It can be expected that if the metal in **2**-Zn-*t,o* is replaced with a variable valent one such as Fe and the distortion of its ring is appropriately increased, a practical heme analog will be born.

Declaration of competing interest

The authors declare that they have no known competing financial interests or personal relationships that could have appeared to influence the work reported in this paper.

Acknowledgments

This study was supported by the Institute of Elemento-organic Chemistry, Nankai University and the Scientific Research Fund of Hunan Provincial Education Department (No. 20A195) and Hunan Provincial Natural Science Foundation of China (No. 2020JJ4292) and the Science and Technology innovation Program of Hunan Province (No. 2021RC5028).

References

[1] T.L. Poulos, Chem. Rev. 114 (2014) 3919–3962.
[2] W.R. Scheidt, C.A. Reed, Chem. Rev. 81 (1981) 543–555.
[3] W. Zhang, W. Lai, R. Cao, Chem. Rev. 117 (2017) 3717–3797.
[4] X. Huang, J.T. Groves, Chem. Rev. 118 (2018) 2491–2553.
[5] J. Luo, Z. Xie, J. Zou, et al., Chin. Chem. Lett. 33 (2022) 4313–4316.
[6] T.A. Clarke, M.J. Edwards, A.J. Gates, et al., Proc. Natl. Acad. Sci. U. S. A. 108 (2011) 9384–9389.
[7] F. Wu, K. Oki, J. Xue, et al., Org. Lett. 24 (2022) 80–84.
[8] A. Stank, D.B. Kokh, J.C. Fuller, R.C. Wade, Acc. Chem. Res. 49 (2016) 809–815.
[9] T.K. Shokhireva, R.E. Berry, E. Uno, et al., Proc. Natl. Acad. Sci. U. S. A. 100 (2003) 3778–3783.
[10] M.S. Shadrina, G.H. Peslherbe, A.M. English, Biochemistry 54 (2015) 5279–5289.
[11] X. Wen, K.M. Patel, B.S. Russell, K.L. Bren, Biochemistry 46 (2007) 2537–2544.
[12] Z. Liang, H. Guo, H. Lei, R. Cao, Chin. Chem. Lett. 33 (2022) 3999–4002.
[13] K.S. Suslick, M.M. Fox, J. Am. Chem. Soc. 105 (1983) 3507–3510.
[14] R.M. Esquerra, R.A. Jensen, S. Bhaskaran, et al., J. Biol. Chem. 283 (2008) 14165–14175.
[15] H.J.S. de Ropp, S. Sham, A. Asokan, et al., J. Am. Chem. Soc. 124 (2002) 11029–11037.
[16] L. Zhong, X. Wen, T.M. Rabinowitz, et al., Proc. Natl. Acad. Sci. U. S. A. 101 (2004) 8637–8642.
[17] K.P. Keep, P. Dasmeh, J. Phys. Chem. B 117 (2013) 3755–3770.
[18] H.B. Dunford, Peroxidases in Chemistry and Biology, CRC Press, Boca Raton, FL, 1991.
[19] D. Nonaka, H. Wariishi, H. Fujii, Biochemistry 48 (2009) 898–905.
[20] S.S. Mansy, J.S. Olson, G. Gonzalez, M.A. Gilles-Gonzalez, Biochemistry 37 (1998) 12452–12457.
[21] J.A. Shelnutt, X.Z. Song, J.G. Ma, et al., Chem. Soc. Rev. 27 (1998) 31–42.
[22] D.E. Bikiel, F. Forti, L. Boechi, et al., J. Phys. Chem. B 114 (2010) 8536–8543.
[23] M.M. Haque, M. Bayachou, J. Tejero, et al., FEBS J 281 (2014) 5325–5340.
[24] S. Amanullah, P. Saha, A. Nayek, M.E. Ahmed, A. Dey, Chem. Soc. Rev. 50 (2021) 3755–3823.
[25] C. Olea, J. Kuriyan, M.A. Marletta, J. Am. Chem. Soc. 132 (2010) 12794–12795.
[26] M. Tang, Y. Yang, S. Zhang, et al., Inorg. Chem. 57 (2018) 277–287.
[27] J. Zhang, M. Tang, D. Chen, et al., Inorg. Chem. 58 (2019) 2627–2636.
[28] Q. Liu, W. Ren, S. Zhang, et al., Chem. Eur. J. 28 (2022) e202103892.
[29] S. Severance, I. Hamza, Chem. Rev. 109 (2009) 4596–4616.

[30] I. Beletskaya, V.S. Tyurin, A.Y. Tsivadze, R. Guilard, C. Stern, Chem. Rev. 109 (2009) 1659–1713.
[31] J.S. Lindsey, Synthesis of meso-substituted porphyrins, in: K.M. Kadish, K.M. Smith, R. Guilard (Eds.), The Porphyrin Handbook, Academic Press, San Diego, 2000, pp. 45–118.
[32] F.F. Shen, Y. Wang, L. Wang, Chin. Chem. Lett. 34 (2023) 107761.
[33] Q. Liu, J. Zhang, M. Tang, et al., Org. Biomol. Chem. 16 (2018) 7725–7736.
[34] D. Reddy, T.K. Chandrashekar, H. Willigen, Chem. Phys. Lett. 202 (1993) 120–126.
[35] A.B.C. Deutman, T. Woltinge, J.M.M. Smits, et al., Molecules 19 (2014) 5278–5300.
[36] J. Bachmann, D.G. Nocera, J. Am. Chem. Soc. 127 (2005) 4730–4743.
[37] S.L. Gac, L. Fusaro, T. Roisnel, B. Boitrel, J. Am. Chem. Soc. 136 (2014) 6698–6715.
[38] A.D. Adler, F.R. Longo, F. Kampas, J. Kim, J. Inorg, Nucl. Chem. 32 (1970) 2443–2445.
[39] J. Bachmann, D.G. Nocera, J. Am. Chem. Soc. 126 (2004) 2829–2837.
[40] Z. Zhou, M. Tang, Q. Liu, X. Zhang, X. Zhou, Eur. J. Inorg. Chem. 2016 (2016) 3585–3591.
[41] M. Punnagai, S. Joseph, G.N.J. Sastry, Chem. Sci. 116 (2004) 271–283.
[42] G. Schiene-Fischer, J. Habazettl, F. Schmid, G. Fischer, Nat. Struct. Biol. 9 (2002) 419–424.
[43] D. Stewart, A. Sarkar, J. Wampler, J. Mol. Biol. 214 (1990) 253–260.
[44] R. Stein, Adv. Prot. Chem. 44 (1993) 1–24.
[45] G. Maheut, A. Castaings, J.L. Pecaut, et al., J. Am. Chem. Soc. 128 (2006) 6347–6356.
[46] I. Tabushi, S. Kugimiya, M.G. Kinnaird, T. Sasaki, J. Am. Chem. Soc. 107 (1985) 4192–4199.
[47] S. Henrich, O.M.H. Salo-Ahen, B. Huang, et al., J. Mol. Recognit. 23 (2010) 209–219.
[48] H.M. Colquhoun, J.F. Stoddart, D.J. Williams, Angew. Chem. Int. Ed. 25 (1986) 487–507.
[49] T.K. Shokhireva, R.E. Berry, E. Uno, et al., Proc. Natl. Acad. Sci. U. S. A. 100 (2003) 3778–3783.
[50] R.M. Esquerra, B.M. Bibi, P. Tipgunlakant, et al., Biochemistry 55 (2016) 4005–4017.
[51] S. Bhunia, A. Ghatak, A. Dey, Chem. Rev. 122 (2022) 12370–12426.
[52] K.M. Lancaster, Biological outer-sphere coordination, in: D.M.P. Mingos, P. Day, J.P. Dahl (Eds.), Molecular Electronic Structures of Transition Metal Complexes I, Springer, Berlin Heidelberg, 2012.
[53] T. Liu, Y. Liu, X. Gao, J. Cao, Chin. Chem. Lett. 34 (2023) 107883.
[54] C. Zhuo, H. Cao, X. Wang, S. Liu, X. Wang, Chin. Chem. Lett. 34 (2023) 108011.
[55] J.S. Derrick, M. Loipersberger, S.K. Nistanaki, et al., J. Am. Chem. Soc. 144 (2022) 11656–11663.
[56] L.R. Widger, C.G. Davies, T. Yang, et al., J. Am. Chem. Soc. 136 (2014) 2699–2702.
[57] S.P. de Visser, Chem. Eur. J. 26 (2020) 5308–5327.
[58] M. Momenteau, C.A. Reed, Chem. Rev. 94 (1994) 659–698.
[59] G.E. Wuenschell, C. TBtreau, D. Lavalette, C.A. Reed, J. Am. Chem. Soc. 114 (1992) 3346–3355.
[60] Z. Zhou, X. Zhang, Q. Liu, et al., Inorg. Chem. 52 (2013) 10258–10263.
[61] Z. Zhou, X. Zhou, Q. Liu, X. Zhang, H. Liu, Org. Lett. 17 (2015) 4078–4081.
[62] Z. Zhou, M. Shen, C. Cao, Q. Liu, Z. Yan, Chem. Eur. J. 18 (2012) 7675–7679.
[63] Q. Liu, M. Tang, W. Zeng, et al., Eur. J. Inorg. Chem. 2016 (2016) 5222–5230.
[64] J.W. Buchler, A. De Cian, J. Fischer, et al., J. Am. Chem. Soc. 108 (1986) 3652–3659.
[65] R.H. Abeles, D. Dolphin, Acc. Chem. Res. 9 (1976) 114–120.
[66] T. Ishizuka, N. Grover, C.J. Kingsbury, et al., Chem. Soc. Rev. 51 (2022) 7560–7630.
[67] P. Dechan, G.D. Bajju, P. Sood, U.A. Dar, J. Mol. Struct. 1183 (2019) 87–99.
[68] C.J. Kingsbury, M.O. Senge, Coord. Chem. Rev. 431 (2021) 213760.
[69] T.D. Brennan, W.R. Scheidt, J.A. Shelnutt, J. Am. Chem. Soc. 110 (1988) 3919–3924.
[70] V. Bandarian, K.A. Pattridge, B.W. Lennon, et al., Nat. Struct. Biol. 9 (2002) 53–56.
[71] S. Al-Karadaghi, R. Franco, M. Hansson, et al., Trends Biochem. Sci. 31 (2006) 135–142.
[72] D. Li, D.J. Stuehr, S.R. Yeh, D.L. Rousseau, J. Biol. Chem. 279 (2004) 26489–26499.
[73] Y. Zhang, K. Ren, L. Wang, L. Wang, Z. Fan, Chin. Chem. Lett. 33 (2022) 33–60.
[74] Z. Zhou, C. Cao, Q. Liu, R. Jiang, Org. Lett. 12 (2010) 1780–1783.
[75] G.K. Jennings, M.H. Hsu, L.S. Shock, E.F. Johnson, J.C. Hackett, J. Biol. Chem. 293 (2018) 11433–11446.